Available online at www.sciencedirect.com
ScienceDirect
International Journal of Multiphase Flow 32 (2006) 1110–1122
International Journal of Multiphase Flow
www.elsevier.com/locate/ijmulflow

Dynamic behaviour of a bubble near an elastic infinite interface

Evert Klaseboer [a], Cary K. Turangan [a], Boo Cheong Khoo [b,c,*]

[a] Institute of High Performance Computing, 1 Science Park Road, # 01-01 The Capricorn, Singapore Science Park II, Singapore 117528, Singapore
[b] Department of Mechanical Engineering, National University of Singapore, 10 Kent Ridge Crescent, Singapore 119260, Singapore
[c] Singapore-MIT Alliance, 4 Engineering Drive 3, Singapore 117576, Singapore

Received 29 May 2005; received in revised form 7 May 2006

Abstract

This paper presents a study to describe the behaviour of a non-equilibrium bubble in a fluid (Fluid 1) that is in contact with another fluid (Fluid 2). Fluid 2 is assumed to incorporate some elastic properties, which are modelled through a pressure term at the fluid–fluid interface. The Laplace equation is assumed to be valid in both fluids and the boundary integral method is employed to simulate the dynamics of the bubble and the fluid–fluid interface. Interesting characteristic phenomena concerning bubble oscillations and the deformation of the fluid–fluid interface are studied for a range of parameters (distance from the fluid–fluid interface, density ratios of the two fluids and elastic properties of Fluid 2). Some of the phenomena observed are jet formation in the bubble, bubble splitting, a ring bubble separating from the main bubble, mushroom-shaped bubbles and the dynamic elevation of the elastic interface. Most of these phenomena are only observed when Fluid 2 possesses some elastic properties (besides the usual formation of a high speed liquid jet). Comparisons with experimental observations confirm the validity of our simulations.

Keywords: Oscillating non-equilibrium bubble; Elastic interface; Boundary integral method

1. Introduction

One of the earliest scientific studies concerning non-equilibrium bubbles was directed towards cavitation bubble erosion on ship propellers by Rayleigh (1917). Another area of interest is in underwater warfare where large explosion bubbles of several meters in radius were studied extensively by, for example, Cole (1948). In both cavitation erosion and underwater explosions, the bubbles deform to produce a high speed liquid jet when they collapse near solid structures or boundaries. When the bubble-induced liquid jet (originating from one surface of the bubble) impacts on the opposite surface of the bubble, an intense blast wave is produced. Both the blast wave and the impinging jet can have devastating effects as they induce stress loading on the

* Corresponding author. Tel.: +65 68742889; fax: +65 67791459.
E-mail address: mpekbc@nus.edu.sg (B.C. Khoo).

0301-9322/$ - see front matter © 2006 Elsevier Ltd. All rights reserved.
doi:10.1016/j.ijmultiphaseflow.2006.05.005

structure, which can lead to material failure; see for example Plesset and Chapman (1971). Violently collapsing bubbles can even emit light (sono-luminescence) under certain conditions as described in Brenner et al. (2002). In the last two decades, the high speed jet impingement and the resulting blast wave have been successfully applied to kidney stone fragmentation (or Shock Wave Lithotripsy); see Coleman et al. (1987), Kodama and Takayama (1998), Delius (2000). It has also been used in several other bio-medical treatments in orthopaedics and pain management. Impacting jets have also been suggested as a means of delivering drugs to a targeted tissue as suggested by Shangguan et al. (1995, 1996) or Fletcher et al. (2002).

The type of boundary in the vicinity of an oscillating bubble seems to be able to influence its behaviour. Besides jet formation towards a solid boundary, a jet has been observed to accelerate away from a free surface by Blake and Gibson (1981), Blake et al. (1987). If the boundary possesses some elastic properties (such as jelly-like materials), recent experimental observations by Brujan et al. (2001a,b) revealed a very complex behaviour of the bubble during its collapse phase. The bubble can even split up into two smaller sub-bubbles; see Gibson and Blake (1982), Shima et al. (1989), Kodama and Tomita (2000) or Tomita and Kodama (2003). Similar behaviour was observed when bubbles were oscillating near a solid surface coated with an elastic material such as rubber (Gibson, 1968; Gibson and Blake, 1982; Blake and Gibson, 1987).

The experimental work of Brujan et al. (2001a), which looked into the behaviour of laser-generated bubbles near a transparent polyacrylamide (PAA) gel with 80% water concentration was probably the first to provide high quality images of a non-equilibrium bubble near an elastic interface using a high speed camera. Interesting phenomena such as bubble splitting, migration of the bubble and jet-like ejection of boundary material were observed. Brujan et al. (2001b) further extended their study by performing a parametric study of the influence of the elastic modulus of the PAA gel/water mixture on the bubble evolution (by changing the ratio of PAA gel and water). Not only are the elastic properties of the gel important, but also the distance of the bubble to the elastic material is found to be a crucial parameter.

An ideal tool to simulate non-equilibrium bubbles is the boundary integral method (BIM) as shown by Blake et al. (1987), Wang et al. (1996a) or Wang and Khoo (2004). Since only the boundaries of the problem need a mesh, tracking these boundaries (such as the bubble interface) is accomplished with more ease than with other conventional methods. Duncan and Zhang (1991), Duncan et al. (1996) simulated an oscillating bubble near an elastic boundary using BIM. Unlike Duncan and Zhang (1991) who modelled the elastic boundary using a finite difference method, Duncan et al. (1996) employed a finite element method to model the elastic boundary.

A new approach, based on the work of Klaseboer and Khoo (2004a), was developed by Klaseboer and Khoo (2004b), which employed a full BIM, both in the fluid containing the bubble (Fluid 1) and inside the elastic material (Fluid 2). The elasticity of the material is represented through a pressure term at the interface between Fluids 1 and 2 (fluid–fluid interface) and the Laplace equation is assumed to be valid for both fluids. Klaseboer and Khoo (2004b) have shown that the interaction of the bubble with the elastic boundary for a range of elasticity parameters yields complex bubble behaviour, similar to those observed experimentally by Brujan et al. (2001a). The influence of the stand-off distance was, however, not investigated by Klaseboer and Khoo (2004b). The present work is therefore intended to address this issue among others and at the same time to perform a parametric study, where also some other phenomena not covered previously in Klaseboer and Khoo (2004b) will be investigated. Both the behaviour of the bubble and the fluid–fluid interface are given particular attention.

This paper is arranged as follows. The theoretical model is presented briefly in Section 2. Results of some numerical simulations are presented in Section 3. Besides some specific comparisons with experimental observations available in literature for both the dynamics of the bubble and the fluid–fluid interface, a short parametric study on bubble behaviour for various parameters is also presented. In Section 4, the conclusions are given.

2. The model

A very brief description of the model will be given here. Suppose two fluids (labelled as '1' and '2') are separated by an interface, referred to as 'fluid–fluid interface' (Fig. 1). Both fluids are assumed to extend to infinity. A non-equilibrium bubble is located in a non-elastic Fluid 1 at a distance H away from the fluid–fluid

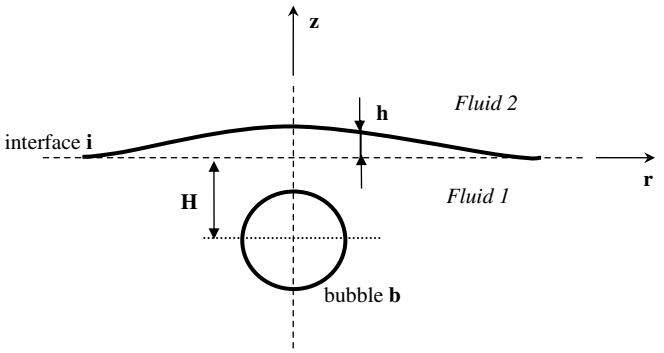

Fig. 1. Schematic outline of the configuration used. A non-equilibrium bubble ***b***, is contained in a non-elastic Fluid 1 that is in contact with an elastic Fluid 2. Both fluids are separated by a fluid–fluid interface *i*. The bubble's centre is initially located at a distance H from the initial equilibrium position of the interface *i* (broken horizontal line). The elevation of the interface *i* during bubble evolution is indicated with h.

interface. H is often referred to as stand-off distance. Fluid 2 may possess some elasticity. The problem under consideration is axisymmetric with the z-axis as the axis of symmetry. The densities of the two fluids, ρ_1 and ρ_2, can be different. Two dimensionless constants characterise the bubble dynamics, the density ratio between Fluids 1 and 2 (α) and the elasticity parameter, (κ) as introduced by Klaseboer and Khoo (2004b). They are given by

$$\alpha = \frac{\rho_1}{\rho_2} \tag{1}$$

and

$$\kappa = \alpha \frac{E}{2(1-\upsilon^2)p_\infty}. \tag{2}$$

Here E is the elastic modulus (or Young modulus) and υ is the Poisson ratio of Fluid 2. For materials that exhibit fluid like behaviour, such as those considered here, $\upsilon = 0.5$. The reference pressure is p_∞ (atmospheric pressure).

For non-dimensionalisation, a suitable scaling factor for lengths is the maximum bubble radius R_m (i.e. the maximum bubble radius in an infinite medium with similar initial conditions). Time t is scaled with $t_0 = R_\mathrm{m}\sqrt{\frac{\rho_1}{p_\infty}}$ and pressure is scaled with p_∞. All variables with a prime are considered dimensionless in this work. The dimensionless parameters for the model are α, κ and

$$H' = H/R_\mathrm{m}. \tag{3}$$

The parameter H' is independent of the properties of both Fluids 1 and 2. On the other hand, the elasticity parameter κ and the density ratio α can be considered as quantities depending only on the two fluids and not on the size or position of the bubble. In this work, the simulations are emphasised on $\alpha \approx 1$ since this value is mostly encountered in bio-medical applications (most biological tissue has a density equal to or close to the density of water, which assumes a magnitude of $\rho_1 = 998\ \mathrm{kg/m^3}$). Effectively, only H' and κ remain as the ranging parameters in this work. The bubble strength ε is defined as the ratio of the initial pressure in the bubble to the reference pressure, i.e.

$$\varepsilon = p_{\mathrm{g}0}/p_\infty. \tag{4}$$

However, as found and discussed in Section 3.4, its influence is not very large. In the present work, $\varepsilon = 100$ with the corresponding initial dimensionless bubble radius $R'_0 = 0.1485$ is employed for most simulations. However, for some examples $\varepsilon = 500$ and $R'_0 = 0.08397$ are used; these examples will be clearly indicated as such.

The numerical implementation is based on potential flow approximations in Fluid 1 and 2. The boundary integral method is applied in both fluids. This will yield a relationship between the potentials and normal

velocities on the interfaces (i.e. bubble and fluid–fluid interface for Fluid 1 and fluid–fluid interface only for Fluid 2). Strictly, the potential flow approximation is not valid in a material with some elastic properties such as Fluid 2. However, in a weakly elastic material, such as studied in the present work, we shall assume that the material still behaves like a fluid. The elasticity of Fluid 2 is taken into account as an extra pressure term across the fluid–fluid interface, which is linearly dependent on the deformation of this interface or h (we introduced h as the elevation of the fluid–fluid interface with respect to its equilibrium position, $h = h(r,t)$). Thus, this pressure term accounts for an additional 'resistance to deformation' in Fluid 2. For low values of κ ($\leqslant 50$) this seems a reasonable approximation, and is deemed so since we are interested in (bio) materials with large water content.

Two boundary conditions are imposed at the fluid–fluid interface. The first is the normal velocity is assumed to be continuous at the fluid–fluid interface. A second boundary condition arises from the pressure difference across the said interface. If the interface is initially planar (equilibrium position) and Fluid 2 incorporates some elastic bulk properties, Klaseboer and Khoo (2004b) have shown that this pressure difference can be expressed as

$$p_1 - p_2 = \frac{E}{2(1-\upsilon^2)R_m} h. \tag{5}$$

Eq. (5) is only valid if Fluid 2 extends to infinity, or in practical terms, is sufficiently 'thick'. This approximation should hold if Fluid 2 is at least a few bubble diameters thick. The pressures p_1 and p_2 can be calculated using the unsteady Bernoulli's equation in both fluids and thus presents a means to relate it to the potentials on the fluid–fluid interface. On the bubble surface, Bernoulli's equation can be used to calculate the potential via the pressure set equal to the internal bubble pressure. The internal pressure of the bubble is assumed to behave adiabatically via

$$p_b' = \varepsilon \left(\frac{V_0'}{V'} \right)^{\gamma}, \tag{6}$$

where V_0'/V' is the volumetric ratio and γ (ratio of specific heats) $= 1.25$. Full details about the numerical method and implementation are given in Klaseboer and Khoo (2004a,b).

In the simulation, when a thin jet develops as the bubble evolves, the computational nodes tend to group together around the jet tip area, which can cause numerical instabilities. An improvement over the numerical scheme employed by Klaseboer and Khoo (2004b) is the implementation of a grid redistribution scheme

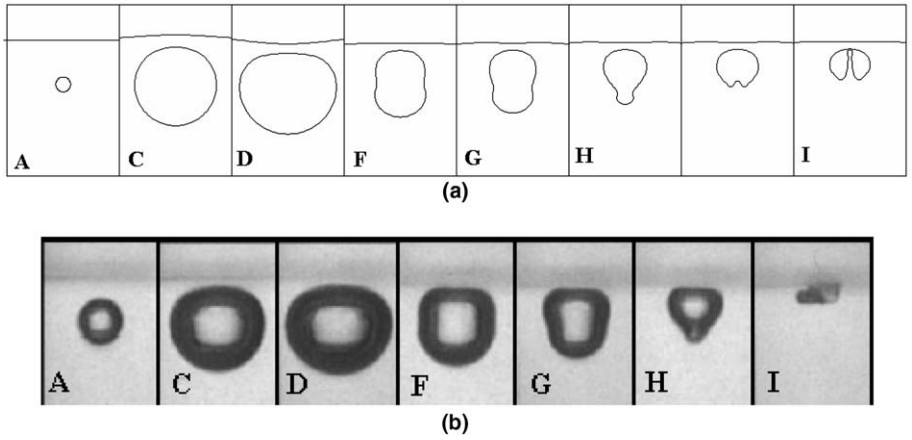

Fig. 2. Comparisons of numerical and experimental results of a non-equilibrium bubble near an elastic interface of PAA/50% water content: $H' = 0.88$ and $\alpha = 0.889$. (a) Numerical simulation with $\varepsilon = 100$, $\kappa = 15$. Individual frame dimension of 2.258 dimensionless width corresponds to the 3.5 mm individual frame width of Fig. 2b. Frame dimensionless times: A at $t' = 0$, C at $t' = 0.411$ (largest deformation of the fluid–fluid interface), D at $t' = 0.902$ (maximum volume of the bubble), F at $t' = 1.710$, G at $t' = 1.770$, H at $t' = 1.855$, $t' = 1.882$ and I at $t' = 1.920$. (b) Experimental observation from Brujan et al. (2001a): A at $t' = 0$, C at $t' = 0.386$, D at $t' = 0.772$, F at $t' = 1.415$, G at $t' = 1.544$, H at $t' = 1.673$ and I at $t' = 1.806$. In the experiment $\kappa = 12.0$ and the maximum bubble radius is $R_m = 1.55$ mm.

identical to the one used by Wang et al. (1996b): after each time step, the bubble surface and the fluid–fluid interface are interpolated using cubic splines. Details on this regridding can be found in Akima (1970). This implementation enables us in certain cases to simulate beyond what was possible in Klaseboer and Khoo (2004b) (see subsequent Fig. 2).

Small bubbles are being considered in our current study, of which the radius is assumed to be in millimetres or below. Buoyancy effects will not have enough time to respond compared to the oscillation time of the bubble, and thus the effect of gravity is negligible. This is verified by calculating the buoyancy parameter given in Klaseboer and Khoo (2004a). On the other hand, the bubbles are sufficiently large for surface tension effects to be negligible as well. Both effects, however, can easily be incorporated into the model if deemed necessary. For all results shown (numerical and experimental), the dimensionless time is set to $t' = 0$ at the moment when the bubble is generated.

3. Results

3.1. Interesting bubble behaviours

Some typical, yet interesting bubble behaviours associated with the oscillation near an elastic membrane are presented here. For an elastic interface with a relatively large elastic parameter κ, a needle-like jet directed towards the fluid–fluid interface is observed. The phenomenon of a so-called neutral collapse with bubble splitting will also be shown. Moreover the separation of a ring shaped bubble separating from the main bubble is simulated. These phenomena were observed in experiments; Brujan et al. (2001a,b), but have not been described in previous numerical simulations.

The current numerical model can simulate the formation of thin high speed jets and avoids node clustering around the jet tip, an event that can cause numerical instabilities. As an example, in Fig. 2a the numerical simulation of a bubble near an elastic interface with $H' = 0.88$, $\alpha = 0.889$ and $\kappa = 15$ is shown. Klaseboer and Khoo (2004b) showed that (in their Fig. 7) the simulation could not be continued beyond the formation of a bubble with a very sharply pointed bottom (i.e. the beginning of the formation of a needle jet directed in the upwards direction). In this pointed region, many nodes were accumulating as the simulation advanced. The advantage of the present enhanced numerical model with node redistribution as mentioned in Section 2 is obvious. In Fig. 2a, the current method can simulate beyond this stage and predicts the formation of the needle jet (between frames 'H' and 'I' as depicted in Fig. 2a during the bubble collapse or contraction phase). In Fig. 2b the corresponding experimental results of Brujan et al. (2001a) are shown. The elastic material of their experiments for this particular case consists of a mixture of 50% polyacrylamide (PAA) and 50% water. The bubble was generated by focusing a laser beam in water. Comparisons show a very good resemblance between the experimental and numerical results. It is important to note that there is no tuning/fudge factor in our model and the dimensionless parameter setting were deduced or justified from the experiment. The corresponding stages of bubble development (viewed in terms of the bubble shapes) are indicated with letters 'A'–'I' in the frames in Fig. 2a and b. Although the timing for the corresponding frames between Fig. 2a and b are not identical, the differences are reasonably small to be about 10% (for example, Frame 'I' appears for $t' = 1.920$ for the numerical results and for $t' = 1.806$ in the experiment). The fluid–fluid interface is not clearly visible due to the specific lighting conditions in this experiment (diffused illumination). It should be noted, however, that the experimental value of $\kappa = 12$ (elastic modulus $E = 2.03$ MPa) was not used, but $\kappa = 15$ was taken instead for the simulations. As explained in Klaseboer and Khoo (2004b), the simulations for $\kappa = 12$ show a very small bubble splitting off at the bottom of the bubble. It was argued there that the numerical model might slightly underestimate the actual value of κ. From a physical point of view, the observed behaviour is very interesting. After its initial growth phase (indicated with 'A'), the bubble expands nearly spherically symmetric ('C'). Subsequently, the interface starts to move downwards towards the bubble ('D'). This leads to a perturbation initiated at the top section of the bubble surface that propagates along the bubble interface ('F' and 'G'). In this particular case, this perturbation is so strong that it travels all the way towards the bottom section of the bubble interface and results in the formation of a very narrow region at the bottom of the bubble ('H'). In a stage between 'H' and 'I' (which are extremely rapid and have not been recorded in the experiments), a high speed needle jet is formed and directed towards the interface. This jet penetrates the bubble and impacts the bubble upper surface nearest the fluid–fluid interface as seen in 'I'.

To investigate the phenomenon of 'bubble splitting', the stand-off distance takes on $H' = 1.22$ in the simulation and the results are depicted in Fig. 3. The elastic interface that consists of a mixture of PAA and 60% water gives an elasticity parameter $\kappa = 6.316$ (using (2) with $E = 1.04$ MPa). The densities of the elastic material and water are $\rho_2 = 1095$ kg/m^3 and $\rho_1 = 998$ kg/m^3, respectively, giving $\alpha = 0.911$, which is near unity. Our simulations are shown in Fig. 3a. Under similar conditions, Brujan et al. (2001b) observed experimentally the 'neutral collapse state' that shows the bubble splitting up into two nearly equal sized bubbles towards the end of the collapse phase (see Fig. 3b, reproduced here for comparison). The most important and interesting features of the simulation are labelled as Frames 'A'–'F'. Fig. 3 clearly shows the formation of two bubbles (''upper'' and ''lower'') with nearly equal size in Frame 'F'. The simulation shows a jet penetrating the lower bubble in the direction away from the upper bubble and eventually impacting on the lower bubble opposite surface. Closer examination of the experimental observation shown in the last two frames of Fig. 3b suggests that the jet tip has penetrated the lower bubble opposite surface. In Fig. 3b, in Frame 'F', it appears that a very thin line is connecting the two bubbles, which might be some fragments of the bubble after the pinching. Similar phenomenon of a 'neutral collapse phase' was also observed by Shima et al. (1989) for a bubble oscillating near a composite surface (bubble splitting is also observed for other values of H', κ and α, and the size of upper and lower portions of the bubble varies depending on the values of these parameters, see Section 3.3 below).

Another interesting phenomenon is the formation of a flat horizontal ring-shaped toroidal bubble separating from the main bubble during its collapse. This is perhaps most clearly observed in the experimental results of Brujan et al. (2001b). In Fig. 4b an experimental bubble evolves near an elastic interface of PAA with 70% water content. In the first two frames shown, the bubble assumes a mushroom-like shape. In the last three frames a horizontal line can clearly be seen. This is associated with the toroidal bubble separating from the mushroom-bubble's ''cap''. This phenomenon also occurred in some other experiments of Brujan et al. (2001a,b). A numerical simulation for this phenomenon is shown in Fig. 4a. Based on the elastic modulus for the material of $E = 0.405$ MPa and the density $\rho_2 = 1073$ kg/m^3, the following parameters are obtained using (1) and (2): $H' = 0.9$, $\kappa = 2.51$ and $\alpha = 0.93$. The numerical simulation has largely captured the

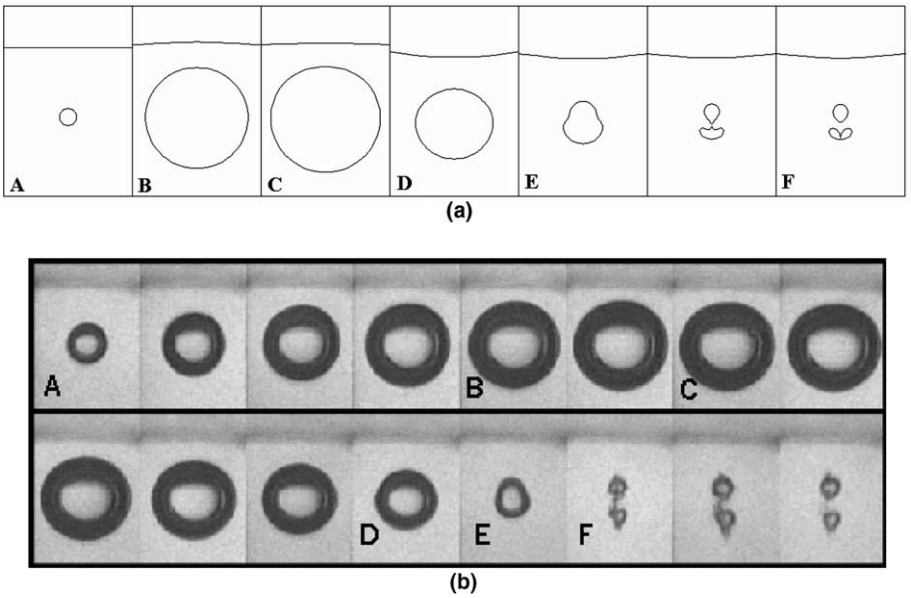

Fig. 3. Comparisons of numerical and experimental results of a bubble near an elastic interface of PAA/60% water content: $H' = 1.22$, $\alpha = 0.911$ and $\kappa = 6.316$ (neutral collapse phase). (a) Numerical simulation with $\varepsilon = 100$. Frame dimensionless times: A at $t' = 0.000$, B at $t' = 0.567$ (largest upwards deformation of the fluid–fluid interface), C at $t' = 0.791$ (near maximum bubble volume), D at $t' = 1.649$, E at $t' = 1.85$, $t' = 1.912$ (bubble splits up in two almost equal parts) and F at $t' = 1.914$ (downwards directed jet developing in lower bubble). (b) Experimental observation from Brujan et al. (2001a). Time interval is 20 μs between two frames (first frame at $t' = 0$, last frame #16 at $t' = 1.93$). The maximum bubble radius is $R_m = 1.55$ mm.

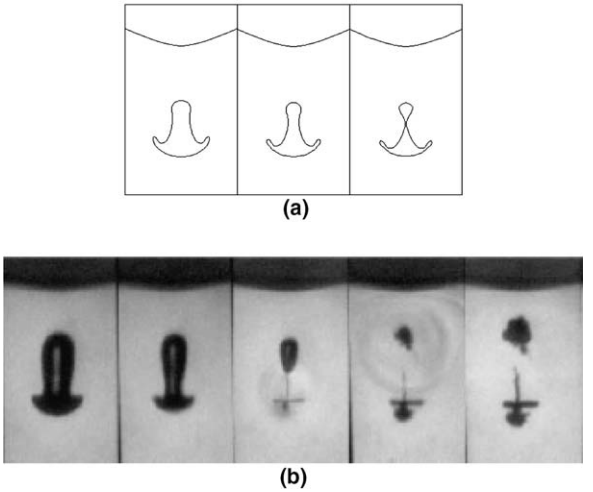

Fig. 4. Typical example of a ring bubble separating from the main bubble. (a) Numerical simulation with parameters: $\varepsilon = 500$, $H' = 0.9$, $\kappa = 2.51$ and $\alpha = 0.930$ (H', κ and α are chosen to match those in the experiment). Frame dimensionless times: Left at $t' = 1.815$, centre at $t' = 1.819$ and light at $t' = 1.822$. (b) Experimental observation from Brujan et al. (2001b). The elastic material is PAA/70% water content. Frame time interval is 1 μs (or $\mathrm{d}t' = 0.00645$ dimensionless) and frame width is 1.4 mm (frame width in numerical results has also been set to match this value). A "ring bubble" is seen here as a horizontal short line above the rounded portion of the bottom of the bubble bottom in the 3rd, 4th and 5th frames from the left. The maximum bubble radius is $R_m = 1.55$ mm.

formation of an elongated mushroom-bubble up to the stage where the top portion of the bubble is about to be separated from mushroom-bubble's cap.

3.2. The evolution of the fluid–fluid interface

The fluid–fluid interface can also exhibit very interesting phenomena. As a typical example, a simulation was performed with $H' = 0.76$ and the results are shown in Fig. 5a. The corresponding experimental results of Brujan et al. (2001a) are shown in Fig. 5b. The elastic material of their experiments consists of a mixture of PAA and 80% water with $E = 0.252$ MPa and $\rho_2 = 1050\ \mathrm{kg/m^3}$, which give the corresponding numerical parameters of $\alpha = 0.95$ and $\kappa = 1.6$. The initial stage at $t' = 0$ is indicated with 'A' in both the numerical and experimental results. As the bubble expands, it pushes the fluid–fluid interface outwards (between Frames 'B' and 'C'). The fluid–fluid interface reaches its maximum elevation at Frame 'C', well before the bubble reaches its maximum volume. Due to a special "*parallel*" illumination technique implemented by Brujan et al. (2001a), the fluid–fluid interface can be distinguished more clearly than in the previous examples. In both the experiment and the numerical simulations, the fluid–fluid interface then retracts back towards its initial position ('C'–'E'). Meanwhile, the bubble assumes a shape with a flattened top. In the next stage ('F'–'I') the fluid–fluid interface moves towards the bubble and the bubble assumes a typical mushroom shape ('I'). Finally, in Frame '*J*' the bubble breaks up in two parts. This typical motion of the fluid–fluid interface towards the bubble, thereby moving quite far from its equilibrium position, has only been observed for fluids with elastic properties (i.e. $\kappa \neq 0$). The physical explanation is probably that a certain amount of elastic energy is stored in Fluid 2, which is then released before the bubble reaches its maximum volume. This behaviour is not only confined to the parameters of Fig. 5, but can be found for a wide range of parameters with $\kappa \neq 0$.

For a more quantitative description, the time–history of the elevation of the fluid–fluid interface at the axis of symmetry, $h'(r' = 0, t')$, is plotted and shown in Fig. 6, where the dimensionless elevation is defined as $h' = h/R_m$. The value of $\alpha = 1$ is chosen in order to eliminate the influence of different densities between Fluids 1 and 2. The bubble is initiated at an initial distance $H' = 1$ away from the fluid–fluid interface. Several parameters of κ have been chosen: ($\kappa = 0$, 0.3, 0.8, 1.5, 2.5, 5, 12 and 50). For $\kappa = 0$ (no elasticity), the fluid–fluid interface returns back to its initial planar shape (equilibrium position) at about $t' = 1.9$. If κ is increased to 0.3, the fluid–fluid interface clearly moves towards the horizontal equilibrium position for times $t' > 1.8$

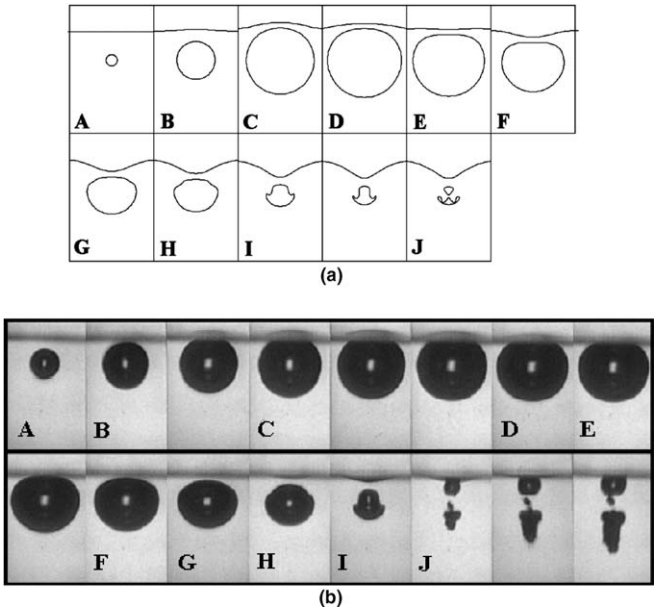

Fig. 5. Comparison of fluid–fluid interface shape, mushroom-shaped bubble and bubble split-up between numerical and experimental results. (a) Numerical simulation with parameters: $\varepsilon = 500$, $H' = 0.76$, $\kappa = 1.6$ and $\alpha = 0.95$. Frame dimensionless times: A at $t' = 0.002$, B at $t' = 0.123$, C at $t' = 0.568$, D at $t' = 0.919$, E at $t' = 1.251$, F at $t' = 1.530$, G at $t' = 1.717$, H at $t' = 1.770$, I at $t' = 1.868$, $t' = 1.893$ and **J** at $t' = 1.918$. (b) Experimental observation using "*parallel*" illumination from Brujan et al. (2001a). The frame time interval is 20 μs (or $\mathrm{d}t' = 0.129$ and thus the last frame is at $t' = 1.935$). The maximum bubble radius is $R_m = 1.55$ mm. Note the clearly visible motion of the fluid–fluid interface.

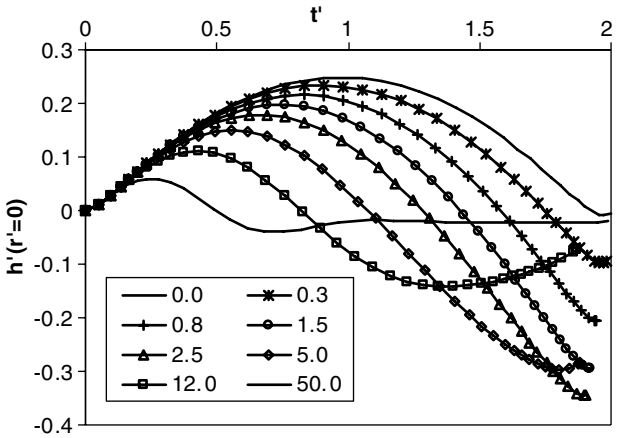

Fig. 6. Plots of the time-histories of the elevation of the fluid–fluid interface at the axis of symmetry $h'(r' = 0)$ for various elasticity parameters κ. Positive elevation means that the fluid–fluid interface is moving upwards from the initial quiescent horizontal axis and away from the bubble, and vice versa. Parameters are $\varepsilon = 100$, $\alpha = 1.0$ and $H' = 1.0$ and κ assumes the values: 0.0, 0.3, 0.8, 1.5, 2.5, 5, 12 and 50.

and overshoots to assume a negative h' value. If κ is further increased, the (first) return to the equilibrium position seems to occur earlier. The maximum positive deflection decreases and also appears to take place at earlier time as κ increases. Overall, the maximum *absolute* minimum deflection occurs for $\kappa = 2.5$ in which $h'(r' = 0, t')$ takes on a negative value of about -0.35. For κ larger than 2.5, the maximum absolute deflection for the fluid–fluid interface decreases again. On the other hand, the maximum positive value of $h'(r' = 0, t')$ decreases monotonically with increasing κ owing to the 'resistance' of the elastic boundary. It only assumes a value of $h'(r' = 0, t') = 0.06$ for $\kappa = 50$ as opposed to $h'(r' = 0, t') = 0.25$ for $\kappa = 0$. The oscillation time of

the fluid–fluid interface, defined as the period from equilibrium position at $t' = 0$ through maximum and minimum elevation and back to the equilibrium position again, appears to increase with increasing κ.

3.3. Parametric study of the interface behaviour for various κ and H'

In Sections 3.1 and 3.2, several interesting phenomena were observed. In this section, we will numerically investigate the behaviour of a bubble near an elastic interface in a more systematic manner and highlight the interesting features. In Fig. 7a, the elasticity parameter κ is plotted on the horizontal axis, and the stand-off distance H' on the vertical axis. The values of H' that are investigated are $H' = 0.5$, 0.75, 1.0, 1.5 and 2.0 and $\kappa = 0.1$, 0.3, 0.5, 0.8, 1.6, 3, 6, 12, 20 and 50. In order not to obscure the obtained results due to the effects of different densities of the Fluid 1 and Fluid 2, their densities have been chosen to be equal with $\alpha = 1.0$. For the more interesting cases, the behaviour of the bubble and the fluid–fluid interface are plotted during the collapse phase around the minimum bubble volume in sub-figures in Fig. 7b and also indicated with corresponding numbers in Fig. 7a. For reference purposes, the times at which each sub-figure is taken are also indicated. For these sub-figures, the initial position of the bubble is always located on the intersection of the dotted lines; similarly the initial position of the fluid–fluid interface is indicated with a broken line and a fixed dimensionless frame with width 2.0 is drawn around each bubble for ease of direct comparison.

In the upper left corner of Fig. 7a, for large H' and small κ, the bubble remains almost spherical during its collapse phase as the fluid–fluid interface has not much influence on the bubble behaviour. This region has been indicated and is bounded by a solid demarcation line in Fig. 7a. A typical example '1' is indicated for $(\kappa, H') = (0.1, 2.0)$. For $\kappa = 0.1$ the bubble appears to split up when H' is decreased to 0.75 or lower. The fluid–fluid interface also deforms more and moves further towards the bubble as H' decreases. The region of 'bubble splitting' has also been broadly demarcated in Fig. 7a and appears mainly for moderate values of κ and H'. In some cases the bubble splits in almost equal parts: $(\kappa, H') = (0.1, 0.75)$ indicated with '2' in Fig. 7a and b, while in others, a larger upper $[(\kappa, H') = (12, 0.75)$ (case '6')] or lower $[(\kappa, H') = (0.5, 1.0)$ (case '3')] bubble splits off. Bubble splitting can be seen in quite a number of cases. The behaviour is not always straightforward, e.g. for $(\kappa, H') = (3.0, 1.5)$ or case '5', the bubble develops a very thin jet directed away from

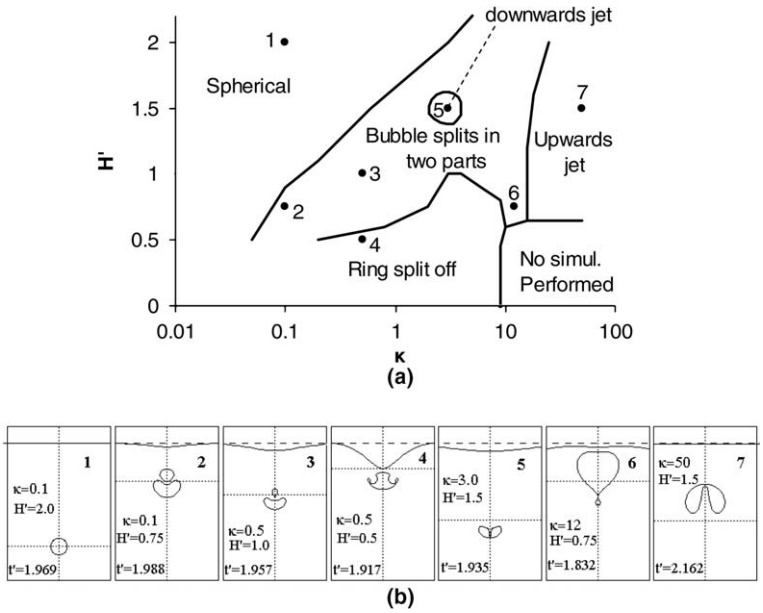

Fig. 7. (a) Parametric study of bubble and interface behaviour for various H' and κ; H' varies from 0.5 to 2.0 and κ from 0.1 to 50. Other parameters: $\varepsilon = 100$ and $\alpha = 1$. The demarcation lines depict three broad regions on bubble characterisation. (b) Some interesting bubble shapes, also indicated with '1'–'7' on Fig. 7a are: '1' spherical collapse; '2', '3' and '6' bubble splitting; '4' ring split-off; '5' downwards jet; and '7' upwards jet.

the fluid–fluid interface. Other simulations with parameters near this particular case at $(\kappa, H') = (1.6, 1.5)$, $(6.0, 1.5)$, $(3.0, 2.0)$ and $(3.0, 1.0)$ depict a break up of the bubble in two separate bubbles. For very large values of κ (>20), a region with a jet directed towards the fluid–fluid interface is seen to appear; as an example case '7' with $(\kappa, H') = (50, 1.5)$ is shown in Fig. 7b. The separation of a ring-shaped bubble from the main bubble occurs mainly for $H' < 1.0$ and $\kappa > 0.5$, but not for $\kappa \gg 6.0$. A typical example '4' is shown for $(\kappa, H') = (0.5, 0.5)$ in Fig. 7b. All the regions mentioned above are broadly demarcated in Fig. 7. A full parametric study with much more details is available directly from the authors.

It is also interesting to note that while keeping H' constant, the fluid–fluid interface deforms most for moderate values of κ, but it hardly moves for $\kappa = 50$. It seems that for larger κ, the fluid–fluid interface behaves more like a solid surface even though the values of κ are still comparatively very small compared to that of say solid aluminium where $\kappa \approx 1.4 \times 10^5$ (obtained via $E = 70$ GPa, $\rho_2 = 2710$ kg/m^3 and $\upsilon = 0.3$ in (1) and (2)).

In general, for lower κ, the bubble tends to move away from the initial quiescent horizontal fluid–fluid interface, whereas for larger κ (especially for $\kappa > 6.0$), the centre of mass of the bubble appears to move towards the said fluid–fluid interface. It should be mentioned, however, that the present simulations are limited to $\kappa \leqslant 6$ for the minimum H' value of 0.5 (this region is also indicated in Fig. 7a). For higher κ, the bubble and fluid–fluid interfaces come close to each other and can lead to numerical instabilities (physically, the dominance of surface science takes precedence which is not accounted for in the present model). The maximum elevation of the fluid–fluid interface during the collapse phase is obtained for $H' = 0.5$ and $\kappa = 1.6$. The fluid–fluid interface even crosses the point where the bubble was initiated on the axis of symmetry for this case.

3.4. Influence of the strength parameter ε

In general, the strength parameter ε does not have a profound influence on the results of the simulations, and therefore $\varepsilon = 100$ has been used for most of our simulations. The larger ε, the smaller the bubble will become in its collapse phase. For example a value of $\varepsilon = 100$, corresponds to an initial dimensionless minimum radius of $R'_0 = 0.1485$. For $\varepsilon = 500$, this reduces to $R'_0 = 0.08397$. The second minimum volume will also be correspondingly smaller for larger values of ε. From the experimental data, for example Fig. 3 of Brujan et al. (2001a), it can be observed that the (second) minimum radius is only about 0.1. In the other experimental cases, the minimum radius is slightly larger (probably also due to the limited time resolution of the camera). As such, values of $\varepsilon = 100$ and 500 are employed in our simulations, lying in the same range as the experiments where most of our comparisons are made.

In certain cases, however, the strength parameter ε can have an influence on the final stage of bubble evolution. This occurs when the simulations are performed near a 'regime' change of the system as indicated in Fig. 7. For example, if the main bubble splits up into a large and very small sub-bubble, a very small change in the parameters could lead to the disappearance of this small bubble. In Fig. 8, such a case is shown for a bubble near an elastic interface with parameters $H' = 1.14$, $\kappa = 1.6$ and $\alpha = 0.95$. In Fig. 8a, $\varepsilon = 100$ whereas in Fig. 8b, $\varepsilon = 500$. The foremost noticeable difference between Fig. 8a and b is that the initial bubble size in Fig. 8b is smaller. As far as bubble shapes are concerned, not much differences can be distinguished between the two simulations during the whole expansion phase. In the collapse phase, the bubbles assume a mushroom shape for both cases. However, the final collapse phase is different as a small bubble splits off for $\varepsilon = 100$ case (Fig. 8a), but no such event is observed in $\varepsilon = 500$ case (Fig. 8b). Nevertheless, a distinct downwards jet develops for both cases. Incidentally, this simulation corresponds to the experimental results of Brujan et al. (2001a) (their Fig. 3a) with an elastic boundary consists of PAA gel with 80% water content. The elastic material has density $\rho_2 = 1050$ kg/m^3 and elastic modulus $E = 0.25$ MPa. The maximum bubble maximum radius is $R_m = 1.55$ mm. Close examination of the last two frames of these experimental results suggests that there is a clear downwards moving jet that can only be identified with a downwards moving 'plume' generated after the downwards jet impacts the bubble opposite surface. The shape of the bubble when it reaches its recorded minimum volume at $t' \approx 1.677$ is rather distorted and it is not clear if a small bubble has been split off or not. In the numerical results, the time for the minimum volume bubble configuration prior to jet impact is slightly different for both strength parameters ε under investigation. For $\varepsilon = 100$ (Fig. 8a) the said time is $t' = 1.941$ whereas for $\varepsilon = 500$ the time is $t' = 1.849$ (Fig. 8b), giving a difference of about 10% when compared to the experimental result.

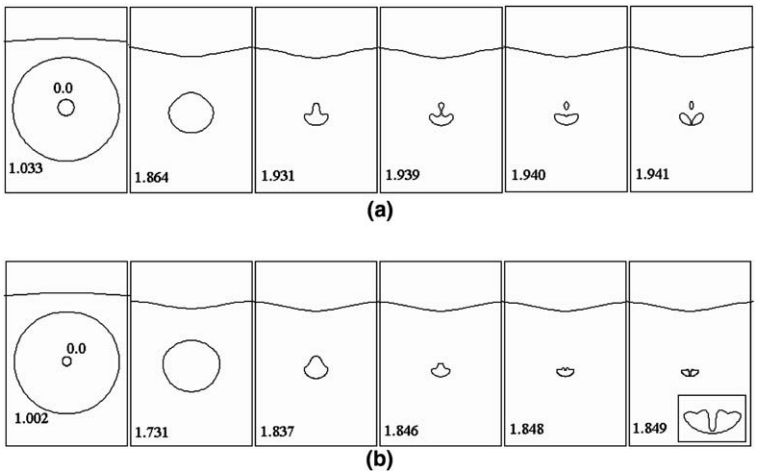

Fig. 8. Comparison of the influence of the strength parameter ε on the bubble shape as a function of time. Simulation parameters: $H' = 1.14$, $\kappa = 1.6$ and $\alpha = 0.95$. (a) Numerical simulation with $\varepsilon = 100$. Frame dimensionless times: $t' = 1.033$ (near maximum volume, the bubble shape at $t' = 0.000$ is also indicated), $t' = 1.864$, $t' = 1.931$, $t' = 1.939$, $t' = 1.940$ and $t' = 1.941$. (b) Numerical simulation with $\varepsilon = 500$. Frame dimensionless times: $t' = 1.002$ (near maximum volume, the bubble shape at $t' = 0.000$ is also indicated), $t' = 1.731$, $t' = 1.837$, $t' = 1.846$, $t' = 1.848$ and $t' = 1.849$ (including a close-up of the bubble shape).

3.5. Perturbation of the interface and pressure contour plots

Klaseboer and Khoo (2004b) showed that a 'perturbation' or 'disturbance' is invariably always initiated near the top section of the bubble nearest the fluid–fluid interface and propagates on the bubble surface for a non-equilibrium bubble oscillating near an elastic interface. The perturbation is believed to be originated from the recovery of the elastic interface near the bubble's maximum size, i.e. the elastic boundary contracting towards its initial equilibrium state. Depending on the values of the parameters H', κ and α, this perturbation can travel around the bubble and be responsible for an impinging jet formation as well as inducing bubble splitting. It appears that in the bubble collapse (or contraction) phase, this perturbation or 'indentation' on the bubble surface is associated with a pressure increase just beside the perturbation region in Fluid 1. As a typical example, the dimensionless pressure plots are shown in Fig. 9 for three instantaneous times ($t' = 1.55$, 1.83 and 1.90) for the case depicted in Fig. 3. The grey regions in Fig. 9a–c indicate the bubble and Fluid 2. The pressure contour plots are only indicated in Fluid 1. In Fig. 9a, the pressure plot is shown at $t' = 1.55$ when the bubble is in its initial collapse phase. The pressure outside the bubble increases rapidly (in the bubble the pressure is the lowest at $p' = 0.22$). A low pressure region outside the bubble is located between the bubble and the fluid–fluid interface. This region is associated with the 'suction' of the elastic Fluid 2, which at this instance has a downwards displacement. At a distance far from the bubble, the dimensionless pressure assumes a value of 1.0. In Fig. 9b, the pressure inside the bubble has increased to $p' = 2.64$, a value well above the reference pressure p'_{ref} of 1.0. Distortions on the bubble surface can be clearly distinguished on the upper sides of the bubble. The regions of Fluid 1 next to the said upper sides of the bubble are associated with high pressure spots with $p' = 3.8$ (since the problem under consideration is axial symmetric, this high pressure region is circular in shape). Far from the bubble, the pressure contour profiles are still nearly spherical except for the region between the bubble and the fluid–fluid interface. Next, in Fig. 9c, the bubble clearly assumes a mushroom shape due to the existence of the distortion on the bubble surface probably caused by the high pressure region in Fluid 1. At this instance, the pressure inside the bubble is $p' = 36.2$, and in a small region just outside the bubble $p' = 40$. The pressure in Fluid 1 surrounding the bubble decreases rapidly for increasing distances from the bubble centre. We found that the example shown in Fig. 9 is quite typical of other simulations which also depicted similar behaviour (results not shown here); invariably in the vicinity of the 'perturbation/disturbance' propagating on the bubble surface is the presence of a localized high pressure region in Fluid 1.

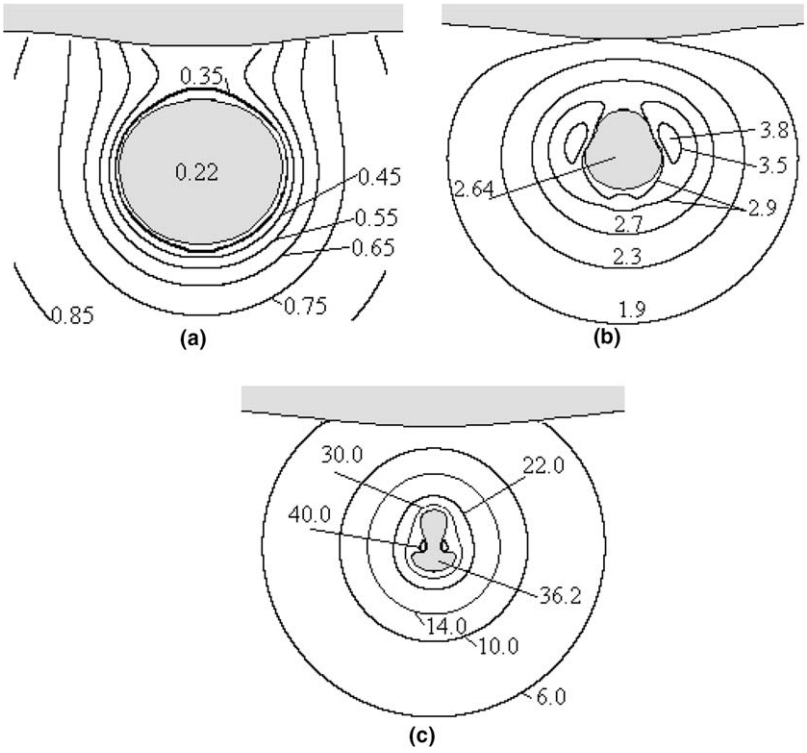

Fig. 9. Iso-pressure contours of the neutral collapse phase of Fig. 3 (numerical parameters are: $\varepsilon = 100$, $H' = 1.22$, $\alpha = 0.911$, $\kappa = 6.316$). In each figure the bubble and Fluid 2 are shaded in grey. (a) $t' = 1.55$; in which the bubble shape is still nearly spherical. Low pressure region is created between the bubble and Fluid 2. (b) $t' = 1.83$; when the bubble shows some 'distortions' on its surface, which is associated with the high pressure region next to the distorted surface and propagates from the top to the bottom section of the bubble. (c) $t' = 1.90$; with the bubble pinching before splitting up. A high pressure region is located just next to the pinching circumference outside the bubble.

4. Discussion and conclusions

A boundary integral method based model was used to simulate the phenomena of an oscillating bubble near an elastic interface and the results have been compared with experimental data. Particular behaviour associated with bubble and fluid–fluid interface include bubble splitting, ring-shaped secondary bubbles separating from the main bubble and the formation of impinging high speed jets directed towards or away from the elastic interface.

In our model, the elastic interface has been modelled as a fluid and its elastic properties have been implemented using a pressure difference across its surface that is in contact with a non-elastic fluid (fluid–fluid interface). The pressure difference is linearly proportional to the elevation of the fluid–fluid interface from its initially planar equilibrium position. A boundary integral method is applied to the non-elastic fluid that contains the bubble (Fluid 1) as well as in the elastic fluid (Fluid 2). The simulations showed that during the interaction of the elastic interface with the bubble, a high pressure region builds up just outside the bubble, which can travel across the bubble's surface as a perturbation of the bubble surface. Depending on the growth of this perturbation and its speed across the bubble surface, the bubble can either split up or form a jet. It is reckoned that the method presented can be developed further and used as a basis to model the bubble behaviour near an elastic interface such as those observed in certain biomedical treatments (e.g. shock wave lithotripsy, shock wave orthopaedics, pain management, etc.).

It may be mentioned that Shaw et al. (1999) studied experimentally a laser-generated bubble near a membrane and observed similar behaviour to that of the present study. In their results, the bubble also assumes a mushroom shape before splitting into two portions. This suggests that the phenomena concerning a bubble oscillating near an elastic boundary (i.e. mushroom shaped bubbles and bubble splitting) also appear when

a bubble oscillates near an elastic membrane. Note also that similar results have been observed experimentally for bubbles oscillating near thin elastic layers, used as coating for solid bodies by Gibson and Blake (1982), Blake and Gibson (1987). The simulations of a non-equilibrium bubble near a thin elastic layer is beyond the scope of the current work since the present model only deals with (semi) infinite elastic materials and not thin layers; this awaits our future study.

References

Akima, H., 1970. A new method of interpolation and smooth curve fitting based on local procedures. J. Assoc. Comput. Mach. 17, 589–602.

Blake, J.R., Taib, B.B., Doherty, G., 1987. Transient cavities near boundaries. Part 2: Free surface. J. Fluid Mech. 191, 197–212.

Blake, J.R., Gibson, D.C., 1981. Growth and collapse of a vapour cavity near a free surface. J. Fluid Mech. 111, 123–140.

Blake, J.R., Gibson, D.C., 1987. Cavitation bubbles near boundaries. Ann. Rev. Fluid Mech. 19, 99–123.

Brenner, M.P., Hilgenfeldt, S., Lohse, D., 2002. Single bubble sonoluminescence. Rev. Mod. Phys. 74, 425–484.

Brujan, E., Nahen, K., Schmidt, P., Vogel, A., 2001a. Dynamics of laser-induced cavitation bubbles near an elastic boundary. J. Fluid Mech. 433, 251–281.

Brujan, E., Nahen, K., Schmidt, P., Vogel, A., 2001b. Dynamics of laser-induced cavitation bubbles near elastic boundaries: influence of the elastic modulus. J. Fluid Mech. 433, 283–314.

Cole, R.H., 1948. Underwater Explosions. Princeton University Press.

Coleman, A.J., Saunders, J.E., Crum, L.A., Dyson, M., 1987. Acoustic cavitation generated by an extracorporeal shock wave lithotripter. Ultrasound Med. Biol. 13, 69–76.

Delius, M., 2000. Lithotripsy. Ultrasound Med. Biol. 26, S55–S58.

Duncan, J.H., Milligan, C.D., Zhang, S., 1996. On the Interaction between a bubble and a submerged compliant structure. J. Sound Vibrat. 197, 17–44.

Duncan, J.H., Zhang, S., 1991. On the interaction of a collapsing cavity and a compliant wall. J. Fluid Mech. 226, 401–423.

Fletcher, D.A., Palanker, D.V., Huie, P., Miller, J., Marmor, M.F., Blumenkranz, M.S., 2002. Intravascular drug delivery with a pulsed liquid microjet. Archives Ophthalmol. 120, 1206–1208.

Gibson, D.C., 1968. Cavitation adjacent to plane boundaries. In: Proceedings of third Australasian Conference on Hydraulics and Fluid Mechanics, Sydney. The Institution of Engineers, Australia, pp. 210–214.

Gibson, D.C., Blake, J.R., 1982. The growth and collapse of bubbles near deformable surfaces. Appl. Sci. Res. 38, 215–224.

Klaseboer, E., Khoo, B.C., 2004a. Boundary integral equations as applied to an oscillating bubble near a fluid–fluid interface. Comput. Mech. 33, 129–138.

Klaseboer, E., Khoo, B.C., 2004b. An oscillating bubble near an elastic material. J. Appl. Phys. 96, 5808–5818.

Kodama, T., Takayama, K., 1998. Dynamic behaviour of bubbles during extracorporeal shock-wave lithotripsy. Ultrasound Med. Biol. 24, 723–738.

Kodama, T., Tomita, Y., 2000. Cavitation bubble behaviour and bubble-shock wave interaction near a gelatin surface as a study of in vivo bubble dynamics. Appl. Phys. B 70, 139–149.

Plesset, M.S., Chapman, R.B., 1971. Collapse of an initially spherical vapor cavity in the neighbourhood of a solid boundary. J. Fluid Mech. 47, 283–290.

Rayleigh, Lord., 1917. On the pressure developed in a liquid during the collapse of a spherical cavity. Phil. Mag. 34, 94–98.

Shangguan, H., Shearin, A., Prahl, S.A., 1995. Visualisation of photoacoustic drug delivery dynamics. Lasers Surg. Med. 57, 4–5.

Shangguan, H., Casperson, L.W., Shearin, A., Gregory, K.W., Prahl, S.A., 1996. Drug delivery with microsecond laser pulses into gelatin. Appl. Opt. 35, 3347–3357.

Shaw, S.J., Jin, Y.H., Gentry, T.P., Emmony, D.C., 1999. Experimental observations of the interaction of a laser generated cavitation bubble with a flexible membrane. Phys. Fluid 11, 2437–2439.

Shima, A., Tomita, Y., Gibson, D.C., Blake, J.R., 1989. The growth and collapse of cavitation bubbles near composite surfaces. J. Fluid Mech. 203, 199–214.

Tomita, Y., Kodama, T., 2003. Interaction of laser-induced cavitation bubbles with composite surfaces. J. Appl. Phys. 94, 2809–2816.

Wang, C., Khoo, B.C., 2004. An indirect boundary element method for three-dimensional explosion problem. J. Comp. Phys. 194, 451–480.

Wang, Q.X., Yeo, K.S., Khoo, B.C., Lam, K.Y., 1996a. Nonlinear interaction between gas bubble and free surface. Comput. Fluids 25, 607–628.

Wang, Q.X., Yeo, K.S., Khoo, B.C., Lam, K.Y., 1996b. Strong interaction between a buoyancy bubble and a free surface. Theor. Comput. Fluid Dynamics 8, 73–88.